ACS OMEGA

Open Access

http://pubs.acs.org/journal/acsodf

Article

Noninvasive Detection of Macrophages in Atherosclerotic Lesions Using a Visipaque-Based Nanoparticle Contrast Agent for Computed Tomography

Shuo Liang, Min Ren, Yanhong Chen, Zhenchun Song, Yapeng Yang, and Hong Zhang*

Cite This: *ACS Omega* 2025, 10, 10979−10986

Read Online

ACCESS | Metrics & More | Article Recommendations

ABSTRACT: This study aimed to evaluate iodinated nanoparticles based on Visipaque for the detection of macrophages in atherosclerotic plaques using computed tomography (CT). The nanoparticles were developed using Visipaque and hydrophobic groups to enhance the macrophages in atherosclerotic lesions. The nanoparticles were measured using NanoSight, and their cellular toxicity was evaluated using the cell counting kit-8 assay. RAW264.7 macrophages were used to detect the cellular uptake of the nanoparticles. Aortic atherosclerotic plaques were induced in New Zealand rabbits (n = 6) by combining a high-cholesterol diet and aortic injury. The noninjured rabbits (n = 4) were fed a normal chow diet and used as controls. CT scans before and 2 h after Visipaque injection, followed by nanoparticle imaging 1 h later. Macrophages were counted using immunohistology with an anti-CD68 monoclonal antibody. The diameter of the nanoparticle agent was approximately 150 mM, and 90% varied broadly between 69 and 248 nm. In vitro experiments demonstrated that the nanoparticles had low cellular toxicity and were effectively endocytosed by macrophages in a time- and dose-dependent manner. In vivo, CT imaging demonstrated that the nanoparticle density was higher in the aortic wall plaques in atherosclerotic rabbits than in control rabbits. The histologic staining confirmed successful atherosclerosis modeling in rabbits and abundant macrophage infiltration in the aortic wall, preferentially taking up the nanoparticles. In conclusion, this study suggests that the novel nanoparticles could be a promising, effective contrast agent for the detection of macrophages in atherosclerotic plaques using CT.

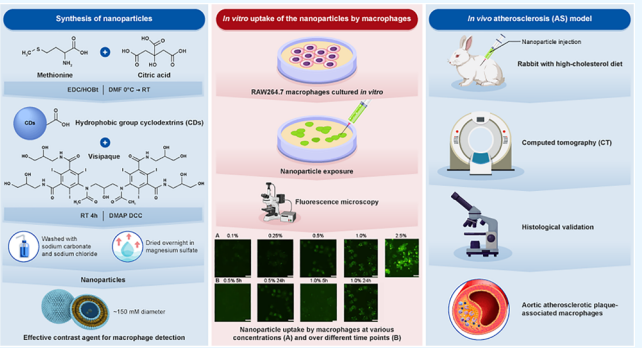

1. INTRODUCTION

Macrophages play a central role in the immune system but also in several pathological processes, including autoimmune diseases and atherosclerosis (AS).[1] In AS, macrophages enter nascent AS lesions, ingest modified lipoprotein particles, and give rise to foam cells.[2,3] Activated macrophages secrete inflammatory cytokines that stimulate smooth muscle cell proliferation and migration and extracellular matrix remodeling, which are critical processes to form necrotic lipid cores, thin fibrous caps, and rupture-prone plaques.[4,5] The disruption of the fibrous cap is a pivotal event that underlies the onset of acute coronary syndrome (ACS) in the majority of patients.[6] Thus, developing an effective noninvasive method to detect the distribution, density, and activity of plaque-associated macrophages may improve the diagnosis and characterization of AS in the future.

Besides its traditional use in imaging, computed tomography (CT) is also a promising molecular imaging instrument that offers high spatial and temporal resolution and has great potential for the detection of AS plaques in coronary arteries.[7,8] In addition, CT imaging is an appealing technique for identifying patients at higher risk of ACS, and CT angiography is an established clinical tool for detecting stenotic lesions in major blood vessels.[9] A CT contrast agent enhances the density and resolution of the target sites to improve the diagnostic efficiency and accuracy of CT imaging.[10] Previous studies showed that the N1177 contrast agent enhanced plaque density and aortic wall imaging in rabbit models of AS.[11,12] However, the mean diameter of the N1177 particles is 259 nm, and macrophages have a higher propensity to engulf particles within the size range of 100 to 200 nm. Therefore, the exploration and development of more appropriate nanoparticle contrast agents for macrophage uptake are required.

An iodinated nanoparticle contrast agent was designed for the CT detection of macrophages in AS plaques. The physical and

Received: October 8, 2024
Revised: February 18, 2025
Accepted: March 10, 2025
Published: March 17, 2025

chemical properties of the nanoparticles were analyzed, followed by testing their cytotoxic and pro-inflammatory effects on macrophages in vitro. The intravenous administration of the agent to rabbits showed accumulation in AS plaques. The study demonstrated the effectiveness of the nanoparticles in detecting macrophage infiltration in AS plaques, offering the potential for AS molecular imaging and therapy monitoring.

2. MATERIALS AND METHODS

2.1. Synthesis and Characterization of the Nanoparticles. The well-characterized Visipaque (320 mg I/ml, GE Healthcare) used for CT imaging was used as the basic material. Then, 3.73 g (25 mmol) of methionine (Sigma-Aldrich) and 4.80 g (25 mmol) of citric acid (Sigma-Aldrich) were dissolved in 110 mL 1:1 DCM/DMF (Sigma-Aldrich). The hydrophobic group cyclodextrins (CDs) were synthesized: 80 mL of dichloromethane (Sigma-Aldrich), 4.74 g of CDs, 3 mL of Visipaque, 4.22 g of DCC (Sigma-Aldrich), and 0.15 g of DMAP (Sigma-Aldrich) were added to a dry 100-ml round-bottom flask and stirred at room temperature for approximately 4 h. After the reaction was complete, the reaction product was washed three times with 20% sodium carbonate solution, washed with saturated sodium chloride solution, dried overnight in waterless magnesium sulfate, and evaporated to obtain the nanoparticles. FT-IR spectrometry was performed to identify the nanoparticles. The size of the nanoparticles was measured using NanoSight (NS300, Malvern Panalytical), a commercial platform for the determination of the size of nanoparticles.

2.2. Cell Viability Assay. The viability of RAW264.7 macrophages treated with the nanoparticles was determined using the Cell Counting Kit-8 Solution Reagent (CCK-8 assay, Beyotime, Nantong). The cells were cultured at a density of 7×10^5 cells per well in 6-well plates. After 24 h, RAW264.7 cells were treated with various concentrations of the nanoparticles nanoparticles or dimethyl sulfoxide (DMSO, Sangon Biotech, A600163-0250). After 24 h, 10 μL of CCK-8 was added to each well, and the cells were incubated at 37 °C for 4 h according to the manufacturer's instructions. Optical density was determined at 450 nm. The relative cell viability from each group relative to controls was determined. The controls only received bovine serum albumin (BSA). All experiments were done in triplicate and repeated three times independently.

2.3. Cellular Uptake of the Nanoparticles. Murine RAW264.7 macrophages (TIANJIN SUOLUOMENBIO) were inoculated in a glass-bottom culture dish for confocal microscopy with a cell density of 1×10^5 cells/well in RPMI 1640 medium (BOSTER, PYG0073) supplemented with 10% fetal bovine serum (LONSERA, S711-001S). The cells were treated with different concentrations of nanoparticles (10, 20, and 40 μg/mL) for 24 h. The nanoparticles were labeled using Alexa Fluor 488 with an excitation wavelength of 488 nm and emission wavelength of 515−545 nm. The cells were observed using a Leica TCS SP8 confocal microscope with an excitation wavelength of 488 nm and a filter of 515−545 nm. The *Z*-axis layer scanning depth was 10 μm, and the layer scanning interval was 0.5 μm. The exposure time was 50 ms, and the frame rate was 5 fps. The images were captured using Leica Application Suite X software to ensure clarity and contrast. ImageJ software was used for image processing, including background deduction, fluorescence intensity quantization, etc. The average fluorescence intensity within each cell was calculated and compared with the control group. The uptake of nanoparticles was quantitatively analyzed using fluorescence intensity and compared with the control group.

2.4. Animal Model. Six male New Zealand White rabbits (mean age, 4 months; mean weight, 2.5 ± 0.2 kg) (BEIJING HFK BIOSCIENCE Co., LTD) were used for AS modeling using a combination of 2 months of a high-cholesterol diet (1.5% cholesterol-enriched diet, 5.0% pork lard and 10% yolk powder (BEIJING HFK BIOSCIENCE Co., LTD)) and an aortic injury created by a single balloon denudation technique (2 weeks after the start of the high-cholesterol diet) to induce aortic AS plaques.[13−15] Before all procedures, the rabbits were anesthetized by an intramuscular injection of xylazine hydrochloride (0.1 mg/kg; Dunhua shengda Animal Health Products Ltd.). Four noninjured rabbits, fed a normal chow diet, were used as controls. Animal experiments and animal care were approved by the Tianjin Chest Hospital of Medicine Institute Animal Care and Use Committee.

2.5. CT Imaging. Before CT images, a 22-gauge catheter (Becton, Dickinson, and Company) connected to a high-pressure syringe (OptiVantge, MALLINCKRODT) was placed in the right marginal ear vein. CT imaging was performed during and 2 h after the intravenous injection of Visipaque (320 mg I/ml, GE Healthcare), at a dose of 2 mL of Visipaque per kilogram of body weight, evaluated with iodixanol at a dose equivalent to 640 mg of iodine per kilogram of body weight. Then, CT imaging was performed again 1 h after nanoparticle injection at a dose of 2 mL per kilogram of body weight. CT angiography was acquired using a 256-slice multidetector CT scanner (Brilliance 256iCT, Philips Healthcare) connected to an ECG simulator (heart rate: 120 times/min). The imaging parameters, adapted from a clinical protocol used for coronary imaging, were as follows: tube voltage, 120 kV; tube current, automatic; rotation time, 330 ms; detector collimation, 128 × 0.625 mm. The field of view was 400 × 100 mm^2, and the data were acquired on a 1024 × 1024 matrix, resulting in a size of 0.625 mm^2. Images were reconstructed by XCB-directed comparison with histology. Scan data were automatically transferred to the postprocessing workstation (PORTAL, Philips Healthcare) for use in multiplanar reconstruction (MPR) image processing.

Considering the dose of 500 mg N1177/kg body weight, the experimental rabbits injected with N1177 received 220 mg of iodine per kilogram of body weight. Given that the nanoparticles in this study were synthesized based on Visipaque and that the rabbits were given an equivalent of 2 mL of Visipaque per kilogram of body weight, evaluated with iodixanol at a dose equivalent to 640 mg of iodine per kilogram of body weight, the experimental rabbits injected with Visipaque received 640 mg of iodine per kilogram of body weight, higher than with N1177.

2.6. Histopathology. The rabbits were euthanized after CT imaging. The heart, liver, and aorta were harvested, weighed, and fixed for 24 h in 4% paraformaldehyde and embedded in paraffin. Then, 5-μm thick sections were cut and matched to CT axial slices as previously described. Sections were stained for lipids (oil red O, Biossci, BP0340) and stained with hematoxylin−eosin (H&E) (Biossci, BP0211). Macrophages were detected by immunohistochemistry using an anti-CD68 antibody antibody [KP1] (Abcam, ab955) as the primary antibody (1:200 dilution) overnight. The secondary antibody was a biotinylated goat antimouse (1:200 dilution) (Zsbio, SPN-9002). The DAB kit (Zsbio, ZLI-9017) procedure was followed, and the slides were imaged with a light microscope.

2.7. Statistical Analysis. The results were expressed as means ± standard deviation (SD). The significance level in all

https://doi.org/10.1021/acsomega.4c09170
ACS Omega 2025, 10, 10979−10986

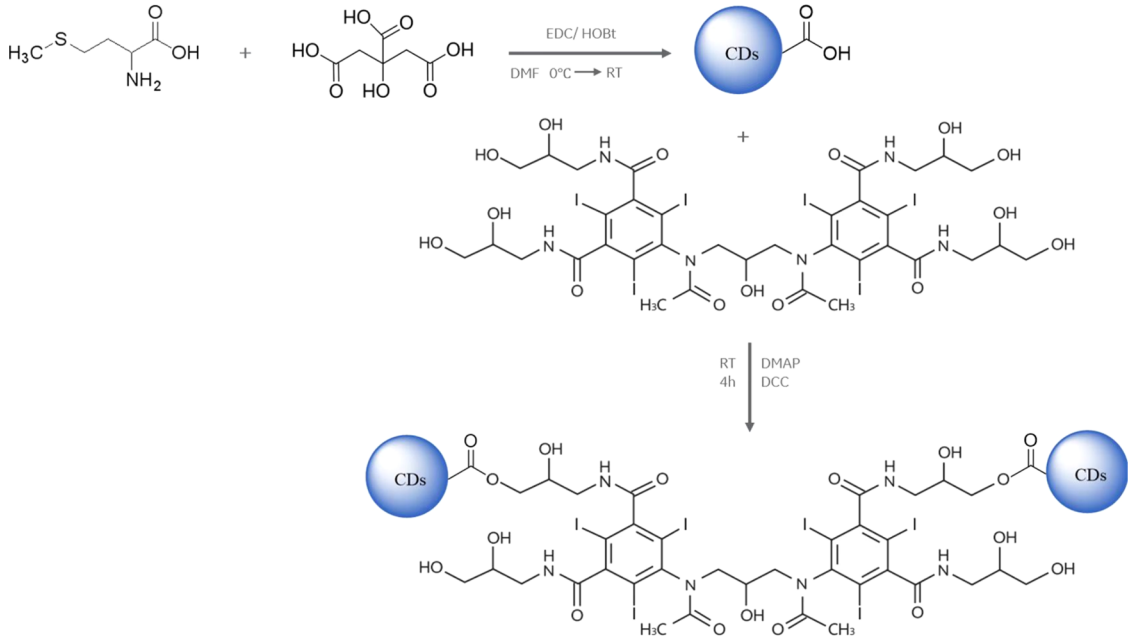

Figure 1. Schematic illustration of the preparation of the nanoparticles.

tests was 0.05. A statistical analysis was conducted using SPSS software to compare the differences between the two groups. All experiments were performed under the regulation and permission of the Animal Care Committee of Tianjin Chest Hospital.

3. RESULTS

3.1. Physicochemical Characterization of Nanoparticle Preparations. A nanoparticle contrast agent based on Visipaque was developed for the detection of macrophages in AS plaques using CT imaging. The structure of the nanoparticles and the synthetic scheme for the nanoparticle contrast are shown in Figure 1. The diameter of the nanoparticles was approximately 150 mM, with 90% of the particles varying broadly in size from 69 to 248 nm (Figure 2A,B). CT scans of saline, Visipaque, and nanoparticle agent showed observable CT attenuation dependent on the formulation of the nanoparticles based on Visipaque (Figure 2C); the CT values of the control, Visipaque, and nanoparticles were 25, 320, and 265 HU, respectively. The nanoparticles remained stable for nearly 5 months. In this study, the lipid solubility of the nanoparticles was increased based on Visipaque, allowing for easy uptake by macrophages. In addition, the nanoparticles had a higher iodide content than N1177, enabling a lower dose for enhanced CT imaging. Altogether, the nanoparticle contrast agent based on Visipaque showed excellent stability and imaging performance for detecting macrophages in AS plaques using CT imaging. These results indicate its promising potential in enhancing the diagnosis of AS in clinical settings.

3.2. In Vitro Uptake of the Nanoparticles by Macrophages. The cytotoxicity of different concentrations of nanoparticles was tested on murine RAW264.7 macrophages in vitro (Figure 2D). After incubation with the nanoparticles at different doses for 12 h, low cytotoxicity was observed for RAW264.7 macrophages when incubated with 1% nanoparticles. No detectable cellular toxicity was found with the nanoparticles for RAW264.7 macrophages when the concentration was <1%. Furthermore, fluorescence microscopy revealed significant differences in the uptake of the nanoparticles by murine RAW264.7 macrophages at various concentrations and at different times. Even at a concentration as low as 0.1%, intracellular fluorescent signals were observed, indicating the propensity of macrophages to endocytose the nanoparticles, consistent with their phagocytic capacity. With the increase in concentration, the most obvious engulfing effect of macrophages was observed at a concentration of 1% of nanoparticles (Figure 3A), suggesting that the endocytosed nanoparticles increased with the probe concentration. In addition, the time-dependent cellular uptake profile of the nanoparticles in macrophages was confirmed (Figure 3B). In conclusion, these results demonstrated that the nanoparticles could be effectively endocytosed by macrophages, which were time- and dose-dependent behavior.

3.3. In Vivo CT Imaging of Plaque-Associated Macrophages. In order to evaluate the availability of using the nanoparticles for AS CT imaging, the nanoparticles were intravenously injected into the rabbits with AS. After a high-cholesterol diet for 2 months and aortic injury, large AS plaques were present in the thoracic aorta of rabbits (Figure 4A), validating the success of the AS model in rabbits. In Figure 4B, a plaque (indicated by the white arrow) is visible in the descending aorta. The aortic lumen shows high density, while the plaque appears to have low density, suggesting a lipid-rich plaque. In Figure 4C, with Visipaque, the density of the aortic lumen decreases, and the plaque in the descending aorta (indicated by the white arrow) remains at a low density, making it more difficult to distinguish from the aortic lumen. In Figure 4D, the density of the aortic lumen increases, and the plaque in the descending aorta (indicated by the white arrow) shows even higher density, indicating increased specific uptake of the nanoparticles by the lipid-rich plaque, leading to an increase in density. The results demonstrate that the nanoparticles exhibited significantly higher CT values, enhancing the intensity of the aortic wall in rabbits with AS.

3.4. Histological Staining. In order to confirm the success of the AS model in rabbits, the arteries, liver, and heart tissues of

https://doi.org/10.1021/acsomega.4c09170
ACS Omega 2025, 10, 10979−10986

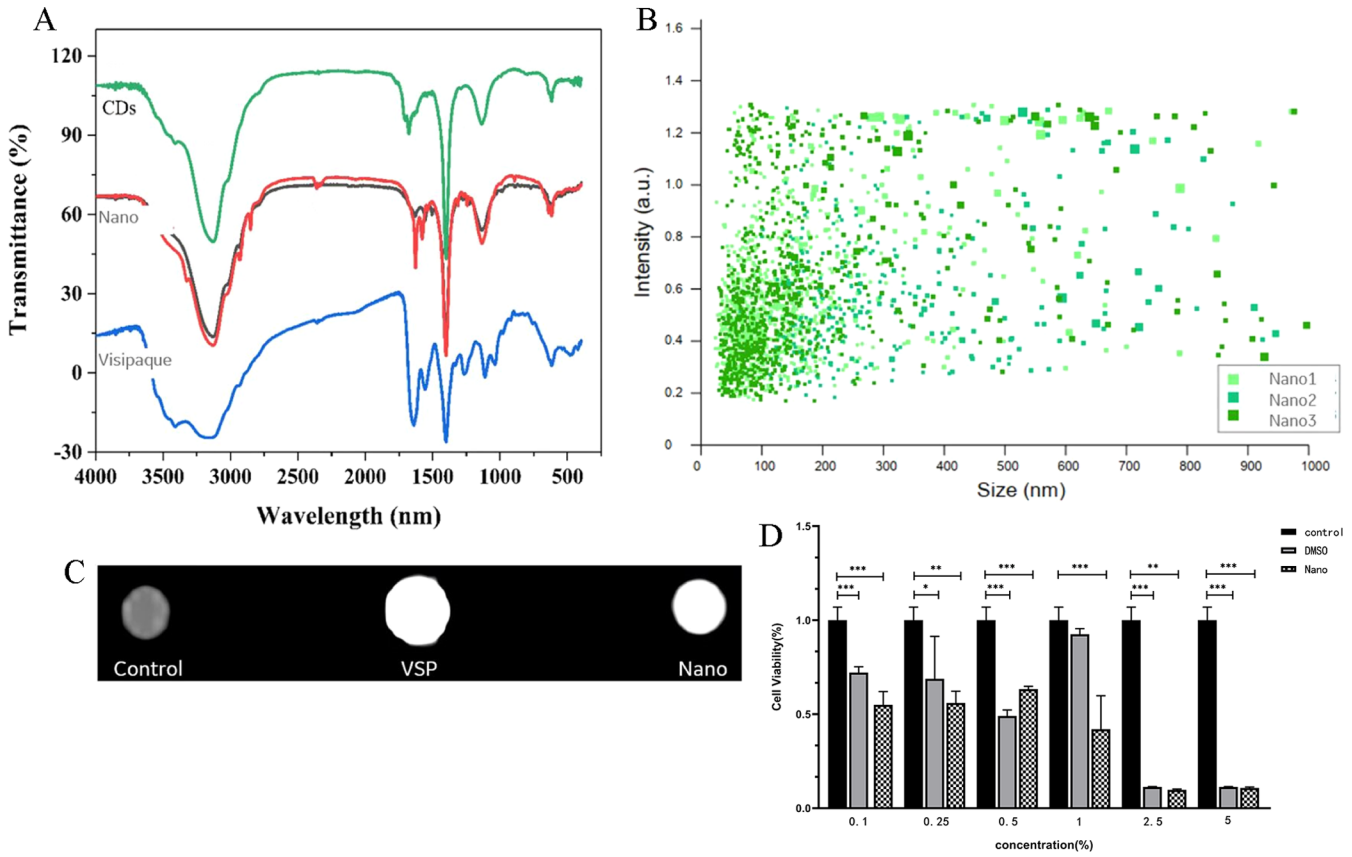

Figure 2. Properties of the nanoparticle contrast agent. (A) Characterization of the nanoparticles identified by FT-IR spectrometry. (B) NanoSight analysis of nanoparticle size. (C) Representative in vitro CT images of saline, Visipaque (VSP), and nanoparticles. (D) CCK-8 assay was performed to evaluate the cell viability of RAW264.7 macrophage cells after treatment with BSA alone or various concentrations of nanoparticles or DMSO. The experiments were conducted in triplicate and repeated independently three times.

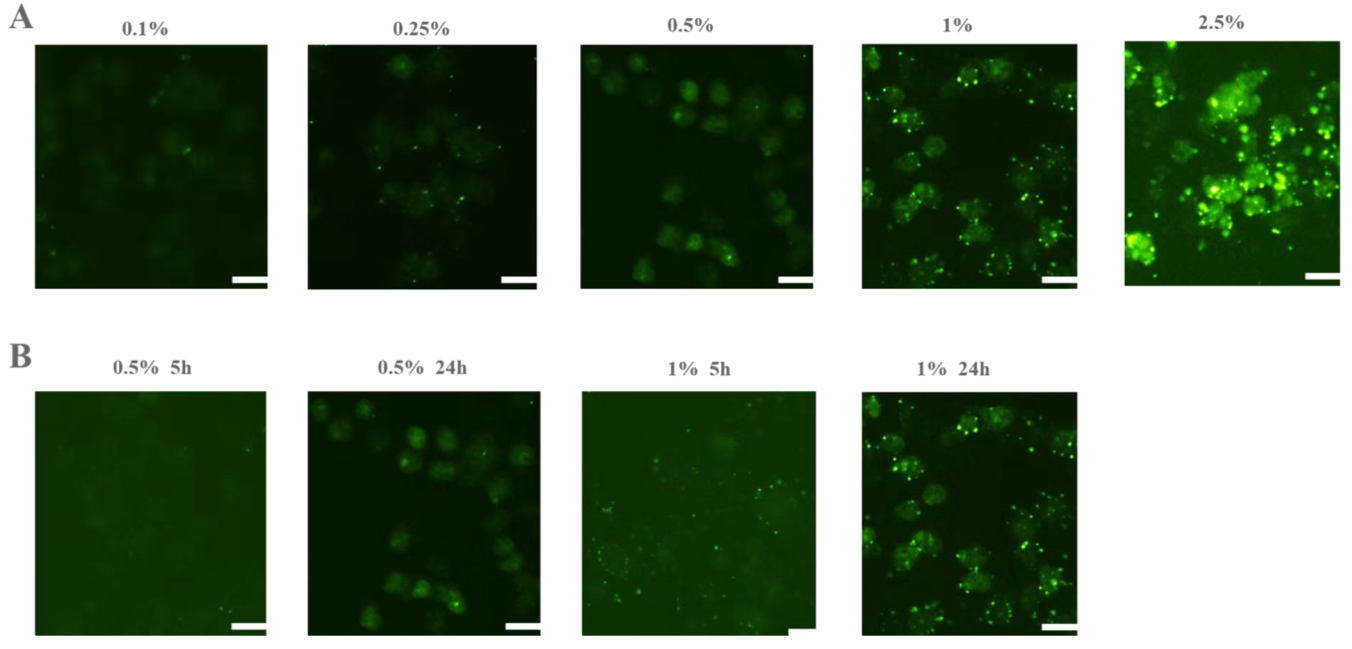

Figure 3. The effect of nanoparticles on cellular uptake of RAW264.7 macrophages. Murine RAW264.7 macrophages were treated with the nanoparticles and observed by fluorescence microscopy to demonstrate the number of signals within the cells. Specifically, we examined the nanoparticle uptake by macrophages at various concentrations (A) and over different time points (B). The scale bar measures 10 μm.

the AS rabbits were subjected to HE staining and oil red O staining. The AS arteries were also stained with the macrophage-specific marker CD68 to investigate the macrophages in AS arteries. Histopathological results of HE and oil red O staining

https://doi.org/10.1021/acsomega.4c09170
ACS Omega 2025, 10, 10979−10986

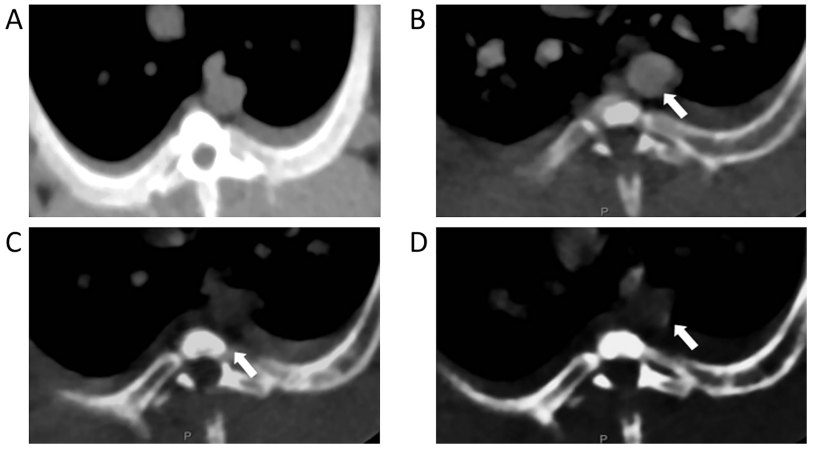

Figure 4. In vivo computed tomography (CT) imaging of plaque-associated macrophages. (A) Scan image before Visipaque (VSP) injection. (B) Image of immediate arterial phase scan after VSP injection. (C) Scan image 2 h after VSP injection. (D) Scan image 1 h after nanoparticles injection.

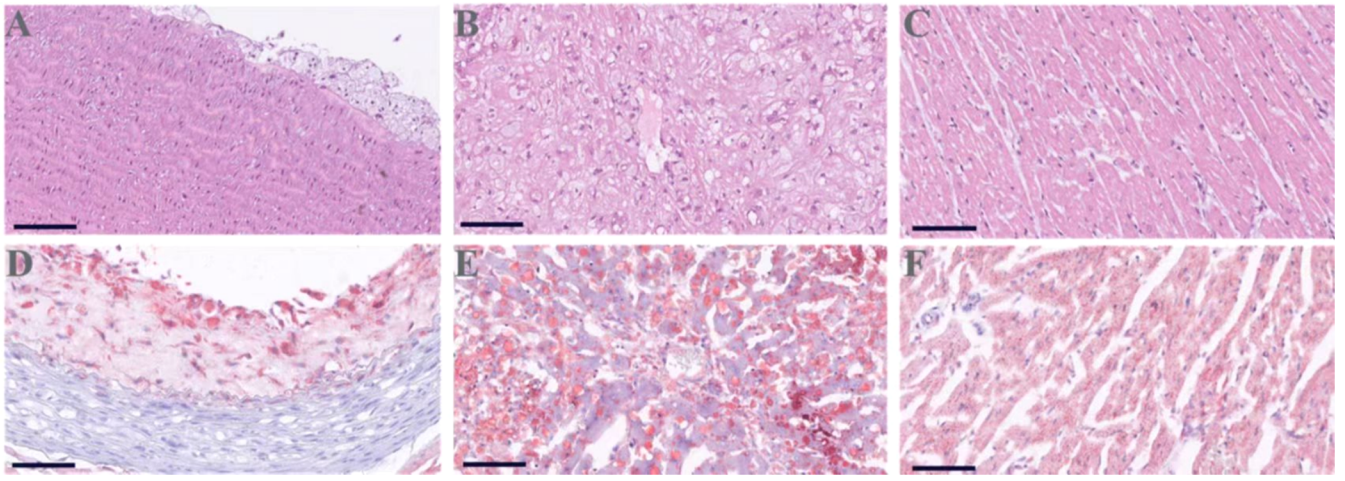

Figure 5. H& E staining and oil red O staining analysis of heart, liver, and aortic tissues in atherosclerosis of rabbits. (A−C). H&E staining of aortic (A), liver (B), and heart (C) tissues in rabbits with atherosclerosis. (D−F). Oil red O staining of aortic (D), liver (E), and heart (F) tissues in rabbits with atherosclerosis. The scale bar measures 100 μm.

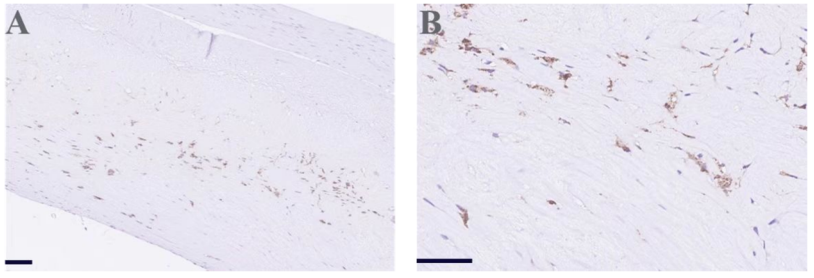

Figure 6. Macrophage infiltration in rabbit model of atherosclerosis. Immunohistochemistry with a monoclonal CD68 antibody (mouse antirabbit macrophage antibody) demonstrated abundant macrophage infiltration in the aortic wall of the aortic in atherosclerosis of rabbits. The images shown are the full view (A) and the magnified version (B), respectively. The scale bar measures 100 μm.

revealed the presence of AS lesions and lipid accumulation within the arterial walls (Figure 5). Additionally, CD68 staining confirmed the abundance of macrophages within the aortic wall and their preferential uptake of the nanoparticles (Figure 6).

4. DISCUSSION

This study showed that the nanoparticles based on Visipaque could be used to detect macrophages in AS plaques using CT. The nanoparticles exhibited favorable characteristics such as stability, low cytotoxicity, and high CT imaging enhancement. The in vitro and in vivo experiments demonstrated the effective uptake of the nanoparticles by macrophages, as well as its potential for accurate CT imaging of AS plaques. These findings suggested a new method for in vivo imaging of macrophages within AS plaques, which can contribute to the early detection and monitoring of AS progression.

In the last two decades, several noninvasive molecular imaging technologies have been used for the detection of AS

https://doi.org/10.1021/acsomega.4c09170
ACS Omega 2025, 10, 10979−10986

plaques.[16−18] The use of ^{18}Ffluoroxyglucose (FDG) for positron emission tomography (PET) imaging is a widely adopted approach for evaluating activated hypoxic macrophages in AS plaques. Nevertheless, nonspecific uptake by metabolically active cells added background signals,[19] limiting its use to image AS plaques. Tarkin et al. reported that PET-CT could identify AS plaques and stratify the risk of rupture using different tracers.[20] PET and SPECT are limited by scanning equipment, reconstruction algorithms, and physical properties. An alternative method involves ultrasmall superparamagnetic particles of iron oxide (USPIO) for magnetic resonance imaging (MRI). The uptake of USPIO by macrophages induces strong T2*-shortening effects, enabling the detection of focal signal voids in AS plaques.[21,22] Despite its potential, challenges persist in precisely quantifying USPIO accumulation due to T1-shortening effects and T2*-effects related to plaque hemorrhage and calcifications.[23]

Recently, diverse imaging modalities and contrast agents have been evaluated for their effectiveness in detecting plaque-associated macrophages,[24] with nanoparticles emerging as promising molecular contrast agents due to their range of magnetic, fluorescent, and radiative properties.[25] Previously, a CT contrast agent named N1177 has been investigated for its efficacy in detecting AS plaques.[12] It is noteworthy that N1177-enhanced MSCT has also shown potential in identifying nonflow-limiting ruptured plaques.[26] However, the hindered transport and delayed clearance attributed to the size of N1177 nanoparticles limited their applicability in detecting macrophage-rich plaques prior to acute events.[12] In the present study, a novel contrast agent utilizing nanoparticles was designed based on Visipaque for the precise detection of macrophages within AS plaques through CT imaging. These nanoparticles possess an average diameter of 150 nm, which falls within the optimal range for efficient macrophage engulfment. CDs are cyclic oligosaccharides consisting of six or more glucose units linked by α-1,4-glucoside bonds.[27,28] Common CDs include α-cyclodextrin (α-CD, six glucose units), β-cyclodextrin (β-CD, seven glucose units), and γ-cyclodextrin (γ-CD, eight glucose units).[27,28] CDs have a hydrophobic inner cavity and a hydrophilic outer surface, so they can form inclusion complexes that enclose hydrophobic molecules in the inner cavity. The hydrophobic inner cavity of CDs can wrap the hydrophobic part of the nanoparticle, thereby enhancing the stability of the nanoparticle and preventing its aggregation in solution.[27,28] CDs improve the dispersion and stability of nanoparticles in solution and ensure their uniform distribution and long-term stability in vivo.[27,28] CDs improve the targeting of nanoparticles since targeting (e.g., antibodies) can be bound to CDs. They also improve the biocompatibility of nanoparticles since the hydrophilic outer surface of CDs can reduce the interaction between nanoparticles and biological tissues and reduce their toxicity.[27,28] Finally, CDs enhance the imaging effect of nanoparticles since they can be combined with imaging reagents.[27,28]

The pivotal role of macrophage uptake in the development of AS is widely recognized.[29] Furthermore, nanoparticles have been reported to expedite their uptake by macrophages in the presence of opsonins.[30] In order to delve deeper into the cellular uptake of nanoparticles by macrophages, in vitro experiments were conducted using murine RAW264.7 macrophages. These experiments revealed that the enhanced lipid solubility of the nanoparticles derived from Visipaque facilitated their efficient uptake by macrophages in a time- and dose-dependent manner. Remarkably, even at a minimal concentration of 0.1%, intracellular fluorescent signals were discernible, thereby leading to significantly improved CT imaging results. These findings substantiate the specific targeting capability of the nanoparticles toward macrophages within AS plaques.

Inflammation is intricately linked to the progression of AS and is profoundly shaped by the involvement of macrophages in this vascular pathology.[31,32] Importantly, the in vitro experiments revealed that the nanoparticles were taken up by macrophages without inducing cytotoxic or pro-inflammatory effects. Moreover, the CT-measured density of the aortic wall exhibited a notable increase 1 h after injection of the nanoparticles to the immediate injection of Visipaque in the same AS rabbit, underscoring the enhanced imaging capability of the nanoparticles for detecting macrophages within AS plaques in vivo. Furthermore, these histologic findings provided further evidence supporting the specific targeting ability of the nanoparticles for macrophages in AS plaques.

It is important to acknowledge the limitations of the study. First, the study only focused on the detection of macrophages in AS plaques and did not explore other cell types or components of the plaques. Second, further investigation into potential toxic effects at higher concentrations may be necessary to understand the safety profile of the nanoparticles. Only the heart and the liver were examined, and possible toxicity to other organs should be investigated. In addition, the long-term stability of the nanoparticles and their potential clearance from the body need to be evaluated in future studies. Nevertheless, it is undeniable that this study strongly suggests the effectiveness and promise of the nanoparticles based on Visipaque for the noninvasive detection of macrophages in AS plaques using CT imaging, which can provide valuable information for clinicians to evaluate AS progression and response to treatment.

5. CONCLUSIONS

This study provided evidence for the effective and safe detection of macrophages in AS using Visipaque-based nanoparticles for CT imaging. Despite some limitations, the findings have significance for the use of nanoparticles as a promising contrast agent for future clinical applications in AS imaging. Further research and improvements are needed to optimize the particle size and enhance the efficiency of macrophage targeting for improved diagnostic and therapeutic interventions in AS.

■ ASSOCIATED CONTENT

Data Availability Statement

All data generated or analyzed during this study are included in this published article.

■ AUTHOR INFORMATION

Corresponding Author

Hong Zhang − *Department of Radiology, Tianjin Chest Hospital, Tianjin 300022, China;* orcid.org/0000-0001-7670-626X; Phone: +86-15822393852; Email: tjch_zhanghong@163.com

Authors

Shuo Liang − *Department of Radiology, Tianjin Chest Hospital, Tianjin 300022, China*

Min Ren − *Department of Radiology, Tianjin Chest Hospital, Tianjin 300022, China*

Yanhong Chen − *Department of Radiology, Tianjin Chest Hospital, Tianjin 300022, China*

https://doi.org/10.1021/acsomega.4c09170
ACS Omega 2025, 10, 10979−10986

Zhenchun Song − *Department of Radiology, Tianjin Chest Hospital, Tianjin 300022, China*
Yapeng Yang − *Department of Radiology, Tianjin Chest Hospital, Tianjin 300022, China*

Complete contact information is available at: https://pubs.acs.org/10.1021/acsomega.4c09170

Author Contributions

S.L. and Y.C. carried out the studies, participated in collecting data, and drafted the manuscript. M.R. and Z.S. performed the statistical analysis and participated in its design. Y.Y. and H.Z. helped to draft the manuscript. All authors read and approved the final manuscript.

Funding

This work was sponsored by the Tianjin Health Research Project [grant number TJSJMYXYC-D2-040].

Notes

The authors declare no competing financial interest.

■ ACKNOWLEDGMENTS

We appreciate Tianjin Chest Hospital for providing strong support for technology, funds, and services.

■ REFERENCES

(1) Zhu, X.; He, L.; Li, X.; Pei, W.; Yang, H.; Zhong, M.; Zhang, M.; Lv, K.; Zhang, Y. LncRNA AK089514/miR-125b-5p/TRAF6 axis mediates macrophage polarization in allergic asthma. *BMC Pulm. Med.* **2023**, *23*, No. 45.
(2) Ye, Z. M.; Yang, S.; Xia, Y. P.; Hu, R. T.; Chen, S.; Li, B. W.; Chen, S. L.; Luo, X. Y.; Mao, L.; Li, Y.; Jin, H.; Qin, C.; Hu, B. LncRNA MIAT sponges miR-149−5p to inhibit efferocytosis in advanced atherosclerosis through CD47 upregulation. *Cell Death Dis.* **2019**, *10*, No. 138.
(3) Yu, X. H.; Deng, W. Y.; Chen, J. J.; Xu, X. D.; Liu, X. X.; Chen, L.; Shi, M. W.; Liu, Q. X.; Tao, M.; Ren, K. LncRNA kcnq1ot1 promotes lipid accumulation and accelerates atherosclerosis via functioning as a ceRNA through the miR-452−3p/HDAC3/ABCA1 axis. *Cell Death Dis.* **2020**, *11*, No. 1043.
(4) Shah, P.; Falk, E.; Badimon, J.; Fernandez-Ortiz, A.; Mailhac, A.; Villareal-Levy, G.; Fallon, J.; Regnstrom, J.; Fuster, V. Human monocyte-derived macrophages induce collagen breakdown in fibrous caps of atherosclerotic plaques. Potential role of matrix-degrading metalloproteinases and implications for plaque rupture. *Circulation* **1995**, *92*, 1565−1569.
(5) Brokopp, C. E.; Schoenauer, R.; Richards, P.; Bauer, S.; Lohmann, C.; Emmert, M.; Weber, B.; Winnik, S.; Aikawa, E.; Graves, K.; Genoni, M.; Vogt, P.; Lüscher, T.; Renner, C.; Hoerstrup, S.; Matter, C. Fibroblast activation protein is induced by inflammation and degrades type I collagen in thin-cap fibroatheromata. *Eur. Heart J.* **2011**, *32*, 2713−2722.
(6) Pello Lázaro, A. M.; Blanco-Colio, L. M.; Franco Peláez, J. A.; Tuñón, J. Anti-Inflammatory Drugs in Patients with Ischemic Heart Disease. *J. Clin. Med.* **2021**, *10*, No. 2835, DOI: 10.3390/jcm10132835.
(7) Bamberg, F.; Sommer, W.; Hoffmann, V.; Achenbach, S.; Nikolaou, K.; Conen, D.; Reiser, M.; Hoffmann, U.; Becker, C. Meta-analysis and systematic review of the long-term predictive value of assessment of coronary atherosclerosis by contrast-enhanced coronary computed tomography angiography. *J. Am. Coll. Cardiol.* **2011**, *57*, 2426−2436.
(8) Han, D.; Berman, D. S.; Miller, R. J. H.; Andreini, D.; Budoff, M. J.; Cademartiri, F.; Chinnaiyan, K.; Choi, J. H.; Conte, E.; Marques, H.; de Araújo Gonçalves, P.; Gottlieb, I.; Hadamitzky, M.; Leipsic, J.; Maffei, E.; Pontone, G.; Shin, S.; Kim, Y. J.; Lee, B. K.; Chun, E. J.; Sung, J. M.; Lee, S. E.; Virmani, R.; Samady, H.; Stone, P.; Narula, J.; Bax, J. J.; Shaw, L. J.; Lin, F. Y.; Min, J. K.; Chang, H. J. Association of Cardiovascular Disease Risk Factor Burden With Progression of Coronary Atherosclerosis Assessed by Serial Coronary Computed Tomographic Angiography. *JAMA Network Open* **2020**, *3*, No. e2011444.
(9) Bai, E. W.; Bennett, J. R.; McCabe, R.; Sharafuddin, M. J.; Bai, H.; Halloran, J.; Vannier, M.; Liu, Y.; Wang, C.; Wang, G. Study of an adaptive bolus chasing CT angiography. *J. Xray Sci. Technol.* **2006**, *14*, 27−38.
(10) Peng, C.; Li, K.; Cao, X.; Xiao, T.; Hou, W.; Zheng, L.; Guo, R.; Shen, M.; Zhang, G.; Shi, X. Facile formation of dendrimer-stabilized gold nanoparticles modified with diatrizoic acid for enhanced computed tomography imaging applications. *Nanoscale* **2012**, *4*, 6768−6778.
(11) Herck, J. L.; De Meyer, G.; Martinet, W.; Salgado, R.; Shivalkar, B.; De Mondt, R.; Van De Ven, H.; Ludwig, A.; Van Der Veken, P.; Van Vaeck, L.; Bult, H.; Herman, A.; Vrints, C. Multi-slice computed tomography with N1177 identifies ruptured atherosclerotic plaques in rabbits. *Basic Res. Cardiol.* **2010**, *105*, 51−59.
(12) Hyafil, F.; Cornily, J.; Rudd, J.; Machac, J.; Feldman, L.; Fayad, Z. Quantification of inflammation within rabbit atherosclerotic plaques using the macrophage-specific CT contrast agent N1177: a comparison with 18F-FDG PET/CT and histology. *J. Nucl. Med.* **2009**, *50*, 959−965.
(13) Lu, H.; Xu, Y.; Zhao, H.; Xu, X. A novel rabbit model of atherosclerotic vulnerable plaque established by cryofluid-induced endothelial injury. *Sci. Rep.* **2024**, *14*, No. 9447.
(14) Phinikaridou, A.; Hallock, K. J.; Qiao, Y.; Hamilton, J. A. A robust rabbit model of human atherosclerosis and atherothrombosis. *J. Lipid Res.* **2009**, *50*, 787−797.
(15) Zhang, G.; Li, M.; Li, L.; Xu, Y.; Li, P.; Yang, C.; Zhou, Y.; Zhang, J. The immunologic injury composite with balloon injury leads to dyslipidemia: a robust rabbit model of human atherosclerosis and vulnerable plaque. *J. Biomed. Biotechnol.* **2012**, *2012*, No. 249129.
(16) Choy, E.; Ganeshalingam, K.; Semb, A. G.; Szekanecz, Z.; Nurmohamed, M. Cardiovascular risk in rheumatoid arthritis: recent advances in the understanding of the pivotal role of inflammation, risk predictors and the impact of treatment. *Rheumatology* **2014**, *53*, 2143−2154.
(17) Varasteh, Z.; De Rose, F.; Mohanta, S.; Li, Y.; Zhang, X.; Miritsch, B.; Scafetta, G.; Yin, C.; Sager, H. B.; Glasl, S.; Gorpas, D.; Habenicht, A. J. R.; Ntziachristos, V.; Weber, W. A.; Bartolazzi, A.; Schwaiger, M.; D'Alessandria, C. Imaging atherosclerotic plaques by targeting Galectin-3 and activated macrophages using ((89)Zr)-DFO-Galectin3-F(ab')(2) mAb. *Theranostics* **2021**, *11*, 1864−1876.
(18) Li, J.; Zheng, L.; Yang, W. J.; Sze-To, C. Y.; Leung, T. W.; Chen, X. Y. Plaque Wall Distribution Pattern of the Atherosclerotic Middle Cerebral Artery Associates With the Circle of Willis Completeness. *Front. Neurol.* **2020**, *11*, No. 599459.
(19) Ogawa, M.; Ishino, S.; Mukai, T.; Asano, D.; Teramoto, N.; Watabe, H.; Kudomi, N.; Shiomi, M.; Magata, Y.; Iida, H.; Saji, H. (18)F-FDG accumulation in atherosclerotic plaques: immunohistochemical and PET imaging study. *J. Nucl. Med.* **2004**, *45*, 1245−1250.
(20) Tarkin, J. M.; Joshi, F.; Rudd, J. PET imaging of inflammation in atherosclerosis. *Nat. Rev. Cardiol.* **2014**, *11*, 443−457.
(21) Jiang, T.; Zhang, C.; Zheng, X.; Xu, X.; Xie, X.; Liu, H.; Liu, S. Noninvasively characterizing the different alphavbeta3 expression patterns in lung cancers with RGD-USPIO using a clinical 3.0T MR scanner. *Int. J. Nanomed.* **2009**, *4*, 241−249.
(22) Huang, C.; Huang, W.; Zhang, L.; Zhang, C.; Zhou, C.; Wei, W.; Li, Y.; Zhou, Q.; Chen, W.; Tang, Y. Targeting Peptide, Fluorescent Reagent Modified Magnetic Liposomes Coated with Rapamycin Target Early Atherosclerotic Plaque and Therapy. *Pharmaceutics* **2022**, *14*, No. 1083, DOI: 10.3390/pharmaceutics14051083.
(23) Trivedi, R. A.; Mallawarachi, C.; U-King-Im, J.; Graves, M.; Horsley, J.; Goddard, M.; Brown, A.; Wang, L.; Kirkpatrick, P.; Brown, J.; Gillard, J. Identifying inflamed carotid plaques using in vivo USPIO-enhanced MR imaging to label plaque macrophages. *Arterioscler., Thromb., Vasc. Biol.* **2006**, *26*, 1601−1606.
(24) Farooq, A.; Sabah, S.; Dhou, S.; Alsawaftah, N.; Husseini, G. Exogenous Contrast Agents in Photoacoustic Imaging: An In Vivo

Review for Tumor Imaging. *Nanomaterials* **2022**, *12*, No. 393, DOI: 10.3390/nano12030393.
(25) Alvieri, F.; Mamani, J. B.; Nucci, M. P.; Oliveira, F. A.; Filgueiras, I. S.; Rego, G. N. A.; de Barboza, M. F.; da Silva, H. R.; Gamarra, L. F. Methods of Granulocyte Isolation from Human Blood and Labeling with Multimodal Superparamagnetic Iron Oxide Nanoparticles. *Molecules* **2020**, *25*, No. 765, DOI: 10.3390/molecules25040765.
(26) Libby, P. Atherosclerosis: disease biology affecting the coronary vasculature. *Am. J. Cardiol.* **2006**, *98*, S3−S9.
(27) Esteso, M. A.; Romero, C. M. Cyclodextrins: Properties and Applications. *Int. J. Mol. Sci.* **2024**, *25*, No. 4547, DOI: 10.3390/ijms25084547.
(28) Poulson, B. G.; Alsulami, Q. A.; Sharfalddin, A.; El Agammy, E. F.; Mouffouk, F.; Emwas, A.-H.; Jaremko, L.; Jaremko, M. Cyclodextrins: Structural, Chemical, and Physical Properties, and Applications. *Polysaccharides* **2022**, *3*, 1−31.
(29) de Gaetano, M.; Alghamdi, K.; Marcone, S.; Belton, O. Conjugated linoleic acid induces an atheroprotective macrophage MΦ2 phenotype and limits foam cell formation. *J. Inflammation* **2015**, *12*, No. 15.
(30) Ding, T.; Sun, J. Mechanistic Understanding of Cell Recognition and Immune Reaction via CR1/CR3 by HAP- and SiO(2)-NPs. *Biomed. Res. Int.* **2020**, *2020*, No. 7474807.
(31) Yang, Q.; Xu, J.; Ma, Q.; Liu, Z.; Sudhahar, V.; Cao, Y.; Wang, L.; Zeng, X.; Zhou, Y.; Zhang, M.; Xu, Y.; Wang, Y.; Weintraub, N. L.; Zhang, C.; Fukai, T.; Wu, C.; Huang, L.; Han, Z.; Wang, T.; Fulton, D. J.; Hong, M.; Huo, Y. PRKAA1/AMPKα1-driven glycolysis in endothelial cells exposed to disturbed flow protects against atherosclerosis. *Nat. Commun.* **2018**, *9*, No. 4667.
(32) Reinhold, S.; Blankesteijn, W. M.; Foulquier, S. The Interplay of WNT and PPARγ Signaling in Vascular Calcification. *Cells* **2020**, *9*, No. 2658, DOI: 10.3390/cells9122658.

https://doi.org/10.1021/acsomega.4c09170
ACS Omega 2025, 10, 10979−10986